Homodyne Detection in Magnetic Resonance Imaging

Douglas C. Noll, Dwight G. Nishimura, *Member, IEEE,* and Albert Macovski, *Fellow, IEEE*

Abstract—**Magnitude detection of complex images in magnetic resonance imaging (MRI) is immune to the effects of incidental phase variations, although in some applications information is lost or images are degraded. Synchronous detection or demodulation, a technique commonly applied to detection of amplitude-modulated signals in communication systems, can be used in MRI systems in place of magnitude detection to provide complete suppression of undesired quadrature components, to preserve polarity and phase information, and to eliminate the biases and reduction in SNR and contrast in low SNR images. The incidental phase variations in an image are removed through the use of a homodyne demodulation reference, a reference that is derived from the image or the object itself. Synchronous homodyne detection has been applied to the detection of low SNR images, the reconstruction of partial *k*-space images, the simultaneous detection of water and lipid signals in quadrature, and the preservation of polarity in inversion-recovery images.**

I. Introduction

MAGNITUDE detection of complex images in magnetic resonance imaging (MRI) has the advantage that it is immune to the effects of incidental phase variations due to RF angle inhomogeneity, filter responses, system delay, noncentered sampling windows, T_2 effects, and in gradient echo sequences inhomogeneity and chemical shift. Additionally, the effects of inhomogeneity and chemical shift are manifest only as geometric distortions or blurring [1], [2]. However, in several applications in MRI, undesired quantities lie 90° out-of-phase (in quadrature) to the desired image. These signals in quadrature can sometimes degrade image quality if presented with a simple magnitude or envelope operator. Additionally, there are applications where information is encoded into the phase or polarity of images. Ability to detect this information is lost with the magnitude operator. Although this information is inherently contained in the in-phase and quadrature channels of the receiver in an MRI system, the incidental and uncontrollable phase variations prevent their use. We present a method, derived from a perspective based on communication theory, to detect these images, thus removing undesired quadrature components or preserving phase and polarity information [3], [4].

Manuscript received May 18, 1990; revised December 12, 1990. This work was supported in part by the GE Medical Systems Group under Contract 22-84, by the National Institutes of Health under Grants HL34962, HL39478, HL39297, and CA50948, and by the National Science Foundation under Contract ECS88-01708.

The authors are with the Magnetic Resonance Systems Research Laboratory, Department of Electrical Engineering, Stanford University, Stanford, CA 94305.

IEEE Log Number 9143048.

II. Method

A. Detection

In communications, the use of envelope detection or equivalently, magnitude detection, is undesirable or results in loss of signal for several cases in amplitude modulation (AM) systems. Given some generalized amplitude modulation signal

$$x_C(t) = [x_i(t) + n_i(t)] \cos(\omega_C t) + [x_q(t) + n_q(t)] \sin(\omega_C t) \quad (1)$$

where

$x_i(t)$	desired and in-phase signal component
$x_q(t)$	quadrature signal component
$n_i(t)$	in-phase noise component (variance = σ^2)
$n_q(t)$	quadrature noise component (variance = σ^2)
$\cos(\omega_C t)$	the carrier.

The detected signal from an envelope or magnitude detector is

$$x_M(t) = \sqrt{(x_i(t) + n_i(t))^2 + (x_q(t) + n_q(t))^2} \quad (2)$$

and if the following conditions are satisfied

$$x_i(t) + n_i(t) > 0 \quad (3)$$

$$\|x_i(t)\| \gg \|x_q(t)\| \text{ or } x_q(t) = 0 \quad (4)$$

$$x_i^2(t) \gg \sigma^2 \quad (5)$$

the detected signal reduces to

$$x_M(t) \approx x_i(t) + n_i(t). \quad (6)$$

This is the desired result since the in-phase component of the noise $n_i(t)$ cannot be distinguished from the desired signal $x_i(t)$. If the carrier $\cos(\omega_C t)$ can be obtained, then a synchronous or coherent detector can be used

$$x_S(t) = \text{LPF}\{x_C(t) \cdot 2\cos(\omega_C t)\} = x_i(t) + n_i(t) \quad (7)$$

where LPF $\{\cdot\}$ is a low-pass filtering function and with no restrictions on the signals or noise.

Similarly, the complex image obtained in an MR experiment can be defined in general as

$$I_C(x, y) = [(m_i(x, y) + n_i(x, y)) + i(m_q(x, y) + n_q(x, y))] e^{i\phi(x,y)} \quad (8)$$

where

$m_i(x, y)$ desired and in-phase signal
$m_q(x, y)$ signal in quadrature to the desired signal
$n_i(x, y)$ in-phase noise component (variance = σ^2)
$n_q(x, y)$ quadrature noise component (variance = σ^2)
$\phi(x, y)$ incidental and uncontrollable phase modulation.

The detected signal from an envelope or magnitude detector is

$$I_M(x, y) = \sqrt{(m_i(x, y) + n_i(x, y))^2 + (m_q(x, y) + n_q(x, y))^2} \quad (9)$$

which again reduces to

$$I_M(x, y) \approx m_i(x, y) + n_i(x, y) \quad (10)$$

when the following conditions are satisfied:

$$m_i(x, y) + n_i(x, y) > 0 \quad (11)$$

$$\|m_i(x, y)\| \gg \|m_q(x, y)\| \text{ or } m_q(x, y) = 0 \quad (12)$$

$$m_i^2(x, y) \gg \sigma^2. \quad (13)$$

We observe that for most MR images, the above conditions (11)–(13) are true. For most imaging sequences, the desired magnetization $m_i(x, y)$ is always positive and has no quadrature components, satisfying the first two conditions. Additionally, most images have a sufficient signal-to-noise ratio (SNR) to satisfy the third condition. In those applications where the above conditions are not true and the incidental phase modulation $\phi(x, y)$ can be determined, then a synchronous detector should be used to demodulate the image

$$I_S(x, y) = \text{Re}\{I_C(x, y)e^{-i\phi(x,y)}\} = m_i(x, y) + n_i(x, y). \quad (14)$$

The synchronous detectors are linear [5], which implies that any filtering of the image or weighting of k space can be done either before or after the detection stage. In addition to the synchronous detector, various other detection schemes can be applied to the complex image to yield similar results with varying degrees of quadrature suppression. Other detectors include the envelope detector with carrier reinsertion [6], which is effectively a linearized envelope detector, and the linearized envelope detector in a balanced configuration. In communications, these detectors are typically used rather than the synchronous detector for ease of implementation, which is not an issue in MRI because the detection is computer implemented. We therefore will consider only the synchronous detector throughout this paper.

B. The Reference

With synchronous detectors in communications, the reference for demodulation can be obtained in several ways, but one common method is to extract the reference from the full spectrum by using a narrow-band filter which passes the carrier cos $(\omega_C t)$ or passes a reference signal from which the carrier can be derived. The carrier is then used to demodulate the AM signal $x_C(t)$. This is known as *homodyne detection* because this carrier is derived from the modulated signal and contrasts to heterodyne demodulation where $x_C(t)$ is demodulated using an independent local oscillator [5]. For accurate demodulation, we require that the carrier be exactly in-phase or coherent with the modulated signal and have adequate SNR. Typically, the first is achieved by design and the latter is satisfied because the narrow-band filter only passes a small amount of noise along with the carrier.

In MRI, the desired image $m_i(x, y)$ is modulated by incidental phase variations $\phi(x, y)$ so for accurate demodulation, the reference should adequately represent these variations. For some generalized reference image:

$$R_C(x, y) = [(r_i(x, y) + n_{r,i}(x, y)) + i(r_q(x, y) + n_{r,q}(x, y))]e^{i\phi(x,y)} \quad (15)$$

where

$r_i(x, y)$ in-phase signal component
$r_q(x, y)$ quadrature signal component
$n_{r,i}(x, y)$ in-phase noise component (variance = σ_r^2)
$n_{r,q}(x, y)$ quadrature noise component (variance = σ_r^2)
$\phi(x, y)$ incidental phase modulation.

The phase reference is then

$$\phi_r(x, y) = \arg R_C(x, y) = \begin{cases} \phi(x, y) + \tan^{-1}\left(\dfrac{r_q(x, y) + n_{r,q}(x, y)}{r_i(x, y) + n_{r,i}(x, y)}\right) & \text{if } r_i(x, y) + n_{r,i}(x, y) > 0 \\ \phi(x, y) + \pi + \tan^{-1}\left(\dfrac{r_q(x, y) + n_{r,q}(x, y)}{r_i(x, y) + n_{r,i}(x, y)}\right) & \text{if } r_i(x, y) + n_{r,i}(x, y) < 0 \end{cases} \quad (16)$$

which reduces to

$$\phi_r(x, y) \approx \phi(x, y) \quad (17)$$

when the following conditions are satisfied:

$$r_i(x, y) + n_{r,i}(x, y) > 0 \quad (18)$$

$$r_q(x, y) = 0 \quad (19)$$

$$r_i^2(x, y) \gg \sigma_r^2. \quad (20)$$

That is, the reference should not be corrupted by polarity shifts, quadrature terms, and noise. In some applications, the reference can be determined by low-pass filtering the

original complex image $I_C(x, y)$ while in other cases, in order to satisfy the above requirements (18)–(20), it may be necessary to collect separately a reference image of the same object. In both cases, object- and sequence-dependent phase variations are demodulated using a reference derived from the same object. For this reason, this technique is also known as *homodyne detection*.

If the reference is to be derived through low-pass filtering, then the filtered image must have approximately the same phase variations as the original complex image. It is commonly observed that the phase in an MR image, while not constant, is often slowly varying. We will show here that if the phase is sufficiently slowly varying, then a low-pass filtered image will have approximately the same phase variations. Neglecting noise, the low-pass filtered image can be written as

$$m_i(x, y)e^{i\phi(x,y)} * g_{lp}(x, y) \tag{21}$$

where $g_{lp}(x, y)$ is the low-pass filtering kernel. If $\phi(x, y)$ varies only slightly over the width of $q_{lp}(x, y)$, then $e^{\phi(x,y)}$ can be pulled outside the convolution

$$m_i(x, y)e^{i\phi(x,y)} * g_{lp}(x, y) \approx [m_i(x, y) * g_{lp}(x, y)]e^{i\phi(x,y)} \tag{22}$$

$$\approx l_i(x, y)e^{i\phi(x,y)} \tag{23}$$

where $l_i(x, y) = m_i(x, y) * g_{lp}(x, y)$, a low-pass filtered version of $m_i(x, y)$. An equivalent condition based on a k-space perspective can be derived using

$$\text{bandwidth } [e^{i\phi(x,y)}] \ll \text{bandwidth } [g_{lp}(x, y)] \tag{24}$$

where bandwidth is measured in k-space.

When the references are acquired separately, care should be taken to ensure that the reference acquisition will result in the same incidental phase variations as the original image $I_C(x, y)$. That is, the sequences should be either both spin echo or both gradient echo sequences. With gradient echos, echo times should be the same, while with spin echos, echo times can be different if constant and linear phase shifts due to timing inaccuracies are determined and removed from the reference. Moreover, since contrast is neither required nor desired, the sequence repetition times can be shortened to reduce reference acquisition time provided changes in eddy current environment are not too severe. As shown above, the phase information can often be determined with a low-pass filtered image. This implies that the reference can be obtained from a low resolution image, requiring only the low order phase encodes, which will further reduce reference acquisition time. Fig. 1 contains a flow diagram for a generalized homodyne detection system.

With phase references derived from low-pass filtered images, errors in the reference may occur when the phase has rapid variations, violating the above conditions (22) and (24). Additionally, noise in the reference and noise correlation between the complex image and the reference may cause errors. These errors and sensitivity of the synchronous detector to these errors will be discussed in a future publication.

III. Applications

A. Noise Reduction

One reason for using a synchronous detector in simple AM is to eliminate the so-called "threshold effect" that occurs in envelope detection of low SNR signals. When the input to the envelope detector is below some threshold SNR, that is, violates the condition in (5), then output SNR is severely degraded [7], [8]. Similarly, when the complex image in MRI has low SNR, magnitude detection can have several deleterious effects. Among these effects are reduced output SNR, reduced contrast, and a noise- and signal-dependent bias in the output mean. These effects are tolerated because generally MR images have sufficient SNR to prevent these threshold effects. In spite of this, poor SNR can arise in images with very late echoes or images with little averaging. Additionally, although parts of images may have good SNR, there may be other parts where the signal is very weak and consequently, will have poor SNR. Another method for addressing these effects is presented in [9].

Given an MR image having poor SNR and no quadrature terms ($m_q(x, y) = 0$), the output of the magnitude operator or detector is

$$I_M(x, y) = \sqrt{[m_i(x, y) + n_i(x, y)]^2 + n_q^2(x, y)} \tag{25}$$

which is described by the Rician distribution [10]. We can define the input and output SNR for a detector

$$\text{SNR}_{\text{in}} = \frac{m_i}{\sigma} \tag{26}$$

$$\text{SNR}_{\text{out}} = \frac{\mu_m - \mu_0}{\sigma_m} \tag{27}$$

where μ_m and σ_m are the mean and standard deviation of I_M with the input signal m_i, and μ_0 is the mean of I_M with no input signal. The relationship between input and output SNR can be approximately determined analytically and is plotted in Fig. 2. The output of the synchronous detector is

$$I_S(x, y) = m_i(x, y) + n_i(x, y) \tag{28}$$

which will have

$$\text{SNR}_{\text{out}} = \frac{m_i}{\sigma} = \text{SNR}_{\text{in}}. \tag{29}$$

The synchronous detector represents the dashed line in Fig. 2.

We can also define a measure of contrast between two levels in an MRI image as

$$C_{\text{in}} = \frac{\Delta m}{m_i} \tag{30}$$

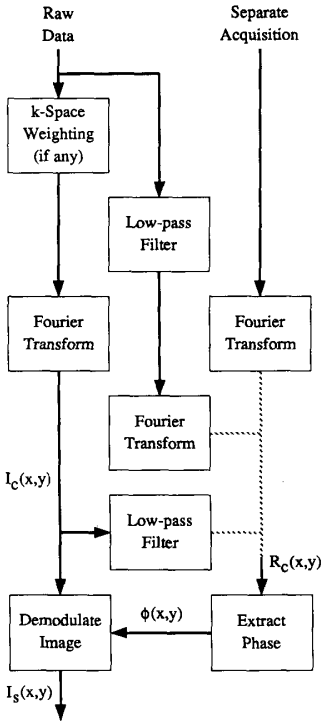

Fig. 1. Flow diagram of a generalized homodyne detection system for MRI showing three possible paths by which the demodulation reference $\phi(x, y)$ can be obtained.

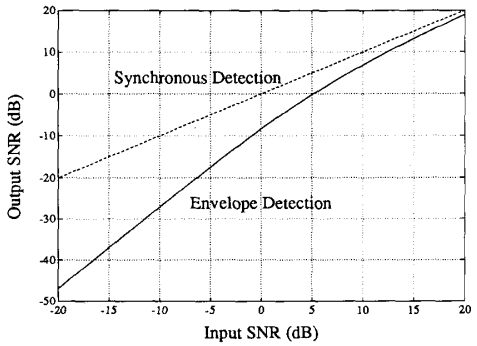

Fig. 2. SNR at the detector output versus SNR at the input for envelope (magnitude) and synchronous detectors.

$$C_{\text{out}} = \frac{\Delta\mu}{\mu_m} \tag{31}$$

for these quantities as defined in Fig. 3. Fig. 4 shows plots of C_{out} for two values of C_{in} plotted versus input SNR m_i/σ. For the envelope detector, these plots show a dramatic reduction of contrast below SNR's of 10 dB and typically contrast is more than halved below SNR's of 0 dB. The synchronous detector, having $C_{\text{out}} = C_{\text{in}}$, shows no degradation in contrast.

Finally, the bias in the mean can cause systematic, noise-, and signal-dependent errors in region-of-interest

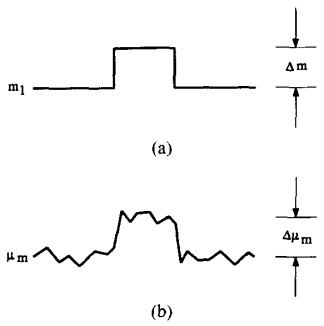

Fig. 3. Quantities for definitions of contrast at: (a) the input and (b) the output.

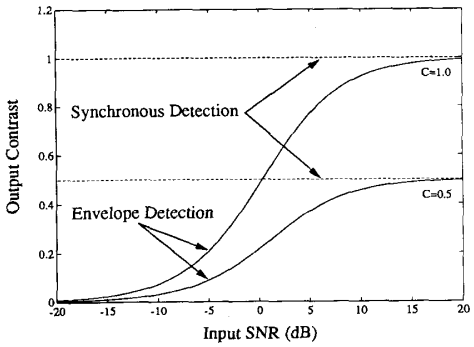

Fig. 4. Contrast at the output of an evelope and synchronous detectors versus input SNR for two values of input contrast.

measurements and T_2 calculations. This bias causes a nonzero mean in areas with no signal, such as airways, bones, and in some sequences, regions where the blood signal has been dephased. Additionally, the bias can lead to incomplete cancellation in techniques like material selective imaging [11] if performed on magnitude images.

These problems at low SNR can be addressed through the use of a synchronous detector. Typically, the reference for demodulation can be obtained by low-pass filtering the low SNR image. This low-pass filtered image will then have sufficient SNR for use as a reference. As previously discussed, if the incidental phase modulation $\phi(x, y)$ varys slowly enough with x and y, then the low-pass filtered reference image will accurately reflect the image phase.

This technique has been applied to a low-SNR, late-echo image of the head of a normal volunteer. The reconstructed image has 256 × 256 pixels over a field of view of 20 cm. The images were acquired at an echo time of 150 ms and repetition time of 1000 ms with no averaging. The demodulation reference was derived by convolving a 5 × 5 rectangular window across the original complex image, which corresponds to a "sinc" low-pass filtering function in k space. The magnitude-detected image is found in Fig. 5(a), and the homodyne-detected image showing improved SNR and contrast is found in Fig. 5(b). The difference of magnitude and homodyne detected im-

(a)

(b)

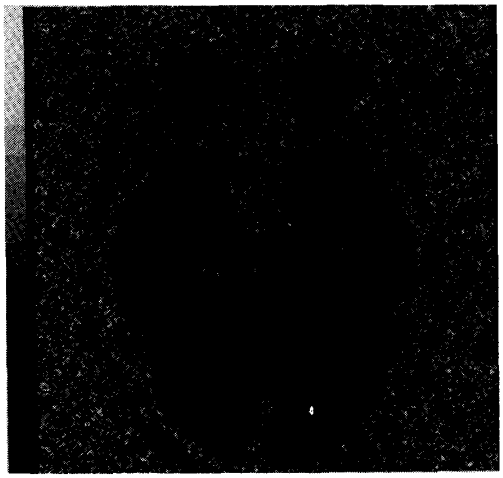

(c)

Fig. 5. (a) Magnitude of a late echo, poor SNR image of the head. (b) Synchronous homodyne detection of the same image demonstrating improved contrast and SNR. (c) Difference of magnitude and homodyne detected images showing the noise that was removed from the magnitude detected image.

TABLE I
SNR AND CONTRAST MEASUREMENTS FOR REGION 1 IN THE LOWER RIGHT OF THE BRAIN AND REGION 2 IN THE CENTER RIGHT OF THE BRAIN AS SHOWN IN FIG. 5

	Homodyne Detection	Magnitude Detection
SNR_1	4.25 dB	0.30 dB
SNR_2	6.95 dB	3.56 dB
$C_{1,2}$	0.32	0.23

ages in Fig. 5(c) shows the noise that was removed from the magnitude detected image. Most of the noise reduction appears to be in regions of air, but some noise is removed from regions of signal. Additionally, other regions of the image show little or no improvement in SNR because these regions have sufficient SNR to prevent the threshold effects.

Measurements of the SNR of (27) are given in Table I for both homodyne and magnitude detection for two regions of the brain as defined in Fig. 5. Table I also contains the contrast of (31) between the same two regions with magnitude detection showing about a 28% reduction in contrast. Differences between these measurements and the theoretical values from Figs. 2 and 4 might be due to the nonhomogeneous nature of the regions.

B. Partial k-Space

Synchronous detection may also be applied to the detection of vestigial side-band (VSB) signals such as those found in commercial television broadcasts. Detection of VSB signals is improved over envelope detection because quadrature terms arising from incomplete sidebands are suppressed. In MRI, the equivalent situation is having incomplete k-space or partial k-space. In practice, partial k-space data sets arise from collecting fewer phase encodes to reduce imaging time while preserving resolution [12], [13]. Partial k-space images also arise from off-center echoes to reduce the minimum achievable echo time and reduce flow and susceptibility dephasing [14], [15]. Several methods of reconstructing partial k-space images have been presented [12], [16]–[20]. Presented here is a method based on the synchronous demodulation of VSB signals, which can be shown to be approximately equivalent to the methods in [12] and [17].

Ignoring noise, we can represent a full k-space image as the superposition of its low and high spatial frequency parts (L and H, respectively)

$$m_i(x, y)e^{i\phi(x,y)} = \mathcal{F}^{-1}\{M(k_x, k_y)\} = \mathcal{F}^{-1}\{L(k_x, k_y) + H(k_x, k_y)\}. \quad (32)$$

Observe that $L(k_x, k_y)$ represents a low-pass filtered version of k space

$$L(k_x, k_y) = M(k_x, k_y) \cdot G_{lp}(k_x, k_y) \quad (33)$$

then, given slowly varying phase

$$\mathcal{F}^{-1}\{L(k_x, k_y)\} \approx l_i(x, y)e^{i\phi(x,y)} \quad (34)$$

by (23). Similarly, observing that

$$H(k_x, k_y) = M(k_x, k_y) - L(k_x, k_y) \tag{35}$$

then the high-frequency part of k space reconstructs to

$$\begin{aligned}\mathfrak{F}^{-1}\{H(k_x, k_y)\} &\approx m_i(x, y)e^{i\phi(x,y)} - l_i(x, y)e^{i\phi(x,y)} \\ &\approx h_i(x, y)e^{i\phi(x,y)}\end{aligned} \tag{36}$$

where $h_i(x, y) = m_i(x, y) - l_i(x, y)$, a real-valued, high-pass filtered version of $m_i(x, y)$. Equation (32) then reduces to

$$m_i(x, y)e^{i\phi(x,y)} = l_i(x, y)e^{i\phi(x,y)} + h_i(x, y)e^{i\phi(x,y)}. \tag{37}$$

For partial k-space having only one-half of the high spatial frequencies, the reconstructed image is

$$\begin{aligned}&\mathfrak{F}^{-1}\{L(k_x, k_y) + u(k_x)\, H(k_x, k_y)\} \\ &\quad = l_i(x, y)e^{i\phi(x,y)} \\ &\qquad + \frac{1}{2} h_i(x, y)e^{i\phi(x,y)} + \frac{1}{2} h_i(x, y)e^{i\phi(x,y)} * \frac{1}{i\pi x}\end{aligned} \tag{38}$$

where $u(\cdot)$ is the unit step function [21]. To compensate for having only half of the high spatial frequency components, those spatial frequencies are doubled and the transformed image is then

$$\begin{aligned}I_C(x, y) &= \mathfrak{F}^{-1}\{L(k_x, k_y) + 2u(k_x)\, H(k_x, k_y)\} \\ &= m_i(x, y)e^{i\phi(x,y)} + h_i(x, y)e^{i\phi(x,y)} * \frac{1}{i\pi x}\end{aligned} \tag{39}$$

where $m_i(x, y)$ is the desired image.

With conventional magnitude detection, the resultant image would be the magnitude of (38). Using synchronous homodyne detection, the resultant image is the demodulated version of (39), which will have the quadrature component suppressed. For partial k-space reconstruction, the demodulation reference is derived by low-pass filtering the original complex image, or equivalently, the reference is derived by reconstructing only the low spatial frequencies

$$R_C(x, y) = \mathfrak{F}^{-1}\{L(k_x, k_y)\} = l_i(x, y)e^{i\phi(x,y)}. \tag{40}$$

The slowly varying condition on $\phi(x, y)$ ensures the reference has proper phase, but also permits simplification of (39). If $\phi(x, y)$ varies only slightly over the region where $\|1/i\pi x\|$ has significant area, then the phase term in (39) can be pulled outside of the convolution

$$h_i(x, y)e^{i\phi(x,y)} * \frac{1}{i\pi x} \approx \left(h_i(x, y) * \frac{1}{i\pi x}\right)e^{i\phi(x,y)} \tag{41}$$

and (39) reduces to

$$I_C(x, y) = \left(m_i(x, y) - ih_i(x, y) * \frac{1}{\pi x}\right)e^{i\phi(x,y)}. \tag{42}$$

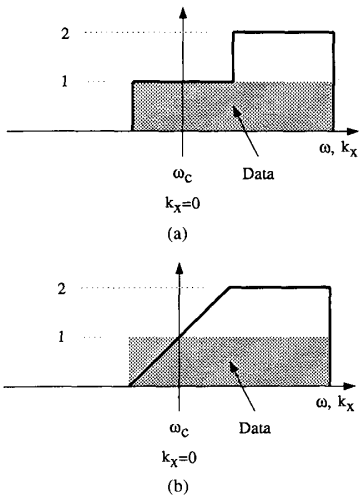

Fig. 6. (a) Step and (b) ramp weighting functions of spectral frequency or k space.

Synchronous detection of this image will now yield just the desired component

$$\begin{aligned}I_S(x, y) &= \text{Re}\,\{I_C(x, y)e^{-i\phi(x,y)}\} \\ &= \text{Re}\left\{m_i(x, y) - ih_i(x, y) * \frac{1}{\pi x}\right\} \\ &= m_i(x, y).\end{aligned} \tag{43}$$

So, with homodyne detection, the image is demodulated so that the desired image lies in the real part and the undesired blurred component lies in quadrature and is discarded.

In (39), the high spatial-frequency data are doubled to account for the lack of high-order negative spatial frequencies. In the detection of VSB signals, the high spatial frequencies are also doubled for the same reason, however, for various practical reasons [22], the spectral weighting is often not the abrupt step weighting as shown in Fig. 6(a). Typically, the chosen filter is a ramp transition from 0 to 2 in the region of the low spectral frequencies as shown in Fig. 6(b). This filter has the property that for any reduction in weighting for one spectral frequency, there is an increase in weighting for the same spectral frequency in the other sideband. Additionally, this filter can be shown to be optimally immune to miscentering of the filter with respect to the carrier ω_C.

Similarly, in MRI, miscentering of the k-space data with respect to the step weighting function and T_2 decay over the readout will cause the effective weighting of spatial frequencies to have abrupt variations. These variations cause artifacts similar in nature to "Gibbs phenomenon" [21] in the images. For this reason, smooth transitions in the weighting function, such as the ramp weighting function, will reduce these artifacts. As in communications, the noise variance can be determined by integrating the square of the weighting function. Table II

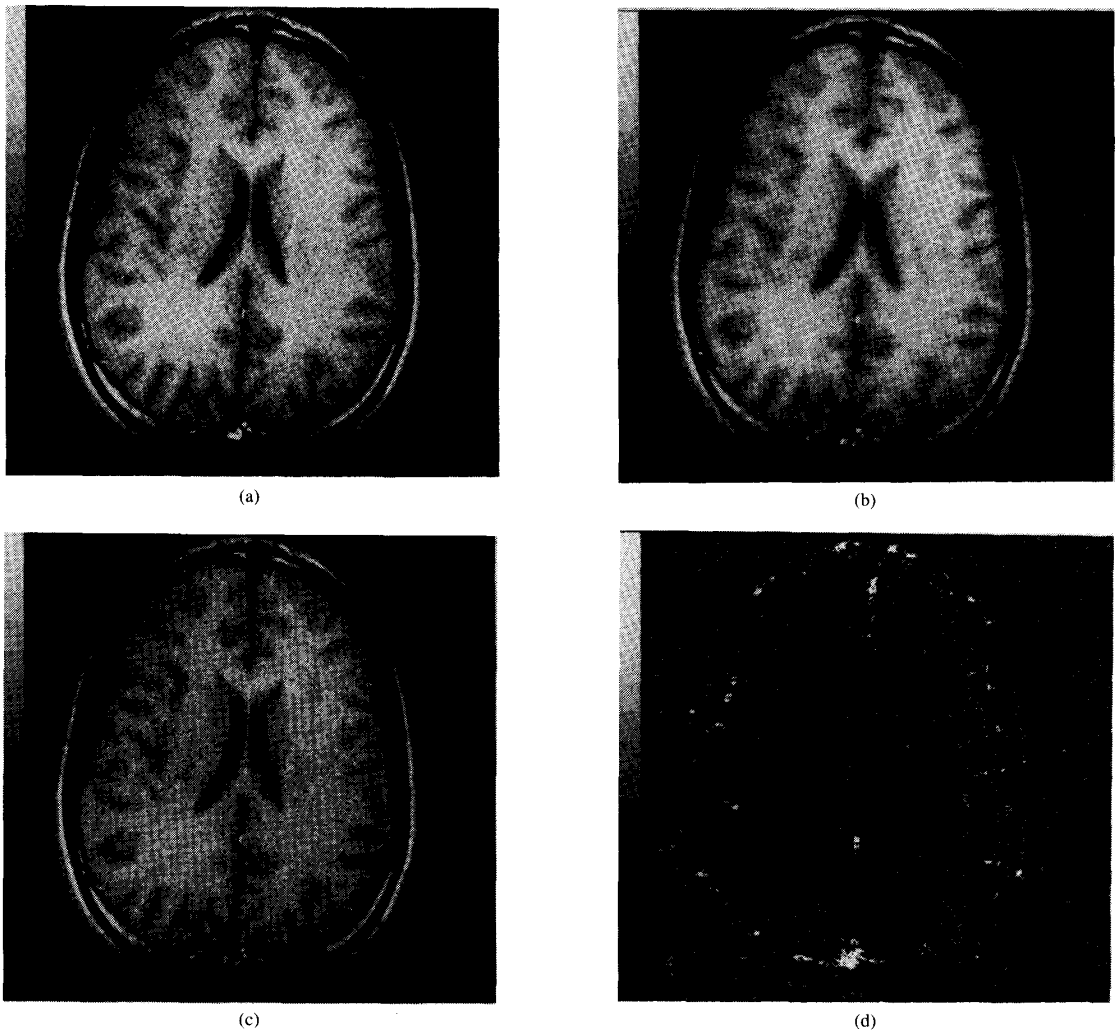

Fig. 7. (a) Magnitude detection of a full k-space, 256 phase-encode image of the head. (b) Magnitude detection of a partial k-space, 144 phase-encode image of the head. (c) Synchronous homodyne detection of the partial k-space image using ramp weighting demonstrating removal of blurring. (d) Difference of full k-space image (a), and synchronous detected partial k-space image (c), showing primarily noise and vessels.

TABLE II
REDUCTION IN SNR FOR WEIGHTED PARTIAL k-SPACE

Fraction of k Space	Reduction of SNR (dB)	
	Step Weighting	Ramp Weighting
$\frac{3}{4}$	1.76	2.22
$\frac{5}{8}$	2.43	2.63
$\frac{9}{16}$	2.73	2.83
$\frac{1}{2}$	3.01	3.01

contains the reduction in SNR for the step and ramp weighting functions when compared to the SNR of the full k-space image.

It can be shown that the step weighting function has optimal noise properties and that suitable weighting functions are bounded by an increase of 3.01 dB. We see that reconstructing partial k-space will result in a reduction of SNR and that reduction of artifacts through the use of a weighting function with smooth transitions will further degrade SNR by a small amount. Other weighting functions with smooth transitions can also be used [17].

We have applied the synchronous homodyne detector, with ramp weighting in k space, to a head image. We used 144 phase encodes ($\frac{9}{16}$ of k space) to reconstruct a 256 $\times$ 256 image. For comparison, an image was constructed from all 256 phase encodes and is found in Fig. 7(a). Magnitude detection, Fig. 7(b), of the unweighted image (38) shows blurring in the direction of the phase encodes (left to right). The homodyne reconstructed image (43) of

Fig. 7(c) shows that the blurring has been removed. The difference between this image and the reference image found in Fig. 7(d) shows primarily noise and vessels, where phase may be rapidly varying.

C. Water–Lipid Separation

Another application for synchronous detection in communications is quadrature carrier multiplexing. In such a system, two channels of information are transmitted 90° out of phase from each other. A synchronous detector is necessary for extraction of the separate channels. A similar method could be used in MR for encoding two species having different resonant frequencies. In particular, water and lipid images can be separately and simultaneously acquired if they are placed 90° out of phase. This can be achieved by displacing the spin echo from the gradient echo by one-fourth of the period of the water–lipid difference frequency τ_{wl} [23]–[25]. This has the advantage over conventional addition–subtraction or Dixon technique water–lipid separation [26] in that only one image needs to be acquired.

The detection of the components can then be done as follows:

$$I_{S,\text{water}}(x, y) = \text{Re}\ \{I_C(x, y)e^{-i\phi(x,y)}\} = m_i(x, y) + n_i(x, y) \quad (44)$$

$$I_{S,\text{lipid}}(x, y) = \text{Im}\ \{I_C(x, y)e^{-i\phi(x,y)}\} = m_q(x, y) + n_q(x, y) \quad (45)$$

where $m_i(x, y)$ contains the water component and $m_q(x, y)$ contains the lipid component. The reference for demodulation, however, cannot be determined from the complex image because the ratio of lipid signal to water signal has been encoded into the phase of the complex image $I_C(x, y)$. The incidental phase here has two components, a system- and sequence-dependent phase and phase accrual due to inhomogeneity

$$\phi(x, y) = \sigma_s(x, y) + \tfrac{1}{4}\tau_{wl}\Delta\omega(x, y) \quad (46)$$

where $\Delta\omega(x, y)$ is the inhomogeneity term. A reference image acquired with spin and gradient echoes together will have all inhomogeneity rephased, will have water and lipid signals aligned, and will therefore contain only the sequence and system dependent phase

$$\phi_1(x, y) = \phi_s(x, y). \quad (47)$$

A second reference image acquired with gradient and spin echoes displaced by τ_{wl}, one full period of the water–lipid difference frequency, will have water and lipid signals aligned as before, but will now have phase due to inhomogeneity in addition to the system and sequence phase

$$\phi_2(x, y) = \phi_s(x, y) + \tau_{wl}\Delta\omega(x, y). \quad (48)$$

From these two images, the inhomogeneity can be determined and then the demodulation reference $\phi(x, y)$ can be calculated from the inhomogeneity and the phase of the first reference image $\phi_1(x, y)$. This method of determining the inhomogeneity is similar to that used in a modified Dixon technique [27].

While this method requires two additional data sets to demodulate the desired image, these do not have to be diagnostic quality images. If the system phase and the inhomogeneity are slowly varying, which they typically are, then the two reference images can be low resolution images, that is, only a few phase encodes need to be collected. Being low resolution, these images will have good SNR and hence little averaging will be required. Additionally, since no particular contrast is desired for the reference images, the repetition time can be reduced to further reduce the acquisition time. For all of these reasons, acquiring the reference images may only slightly increase the total scan time.

Fig. 8(a) shows magnitude detection of the legs from a complex image containing the two components in quadrature showing both water and lipids together. Fig. 8(b) and (c) shows synchronous detection of water and lipid images of the same complex image. The reference images for the detection were constructed only from 32 low spatial frequency phase encodes.

D. Bipolar Inversion Recovery

Double-sideband, suppressed-carrier amplitude modulation (DSB–SC) is still another application of synchronous detection in communications. Envelope detection cannot be used for DSB–SC transmissions because the input signal is not restricted to being positive, that is, it violates the condition of (3). Synchronous detection preserves this polarity information. In MRI, inversion-recovery sequences are used to get excellent T_1 contrast, however, at some inversion times, species having short T_1's will have positive magnetization and species having longer T_1's will have negative magnetization [28]. In a magnitude image, these negative regions appear as positive thus reducing contrast, while in synchronous detection these polarities are preserved. Several other methods of correctly presenting polarity in MR images have been suggested [29]–[31].

As in the water–lipid separation case, the original image cannot be used as the reference due to the polarity shifts that violate the condition in (18). A separately-acquired reference image could also be used to demodulate the image. As before, the reference image can be acquired quickly by reducing repetition time, number of phase encodes, and low averaging. The reference image should not be acquired with an inversion-recovery sequence because phase jumps due to polarity changes corrupt the reference. Synchronous homodyne detection has been applied to an inversion-recovery image and is compared to magnitude detection of the same image in Fig. 9. The original image had 128 phase encodes with T_I = 300 ms and T_R = 1000 ms, while the reference was reconstructed with 32 phase encodes at a T_R = 350 ms with no inversion. The synchronous detection preserves signal polarity and restores the intended contrast.

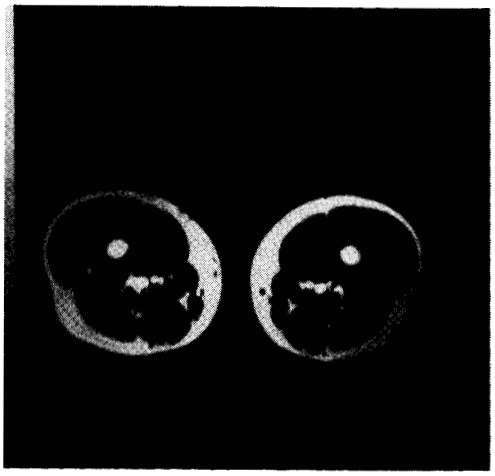

(a)

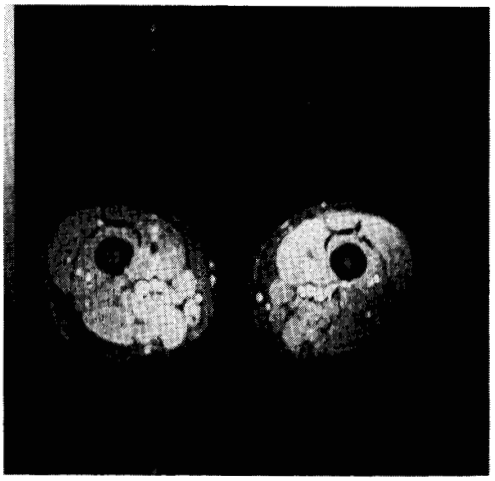

(b)

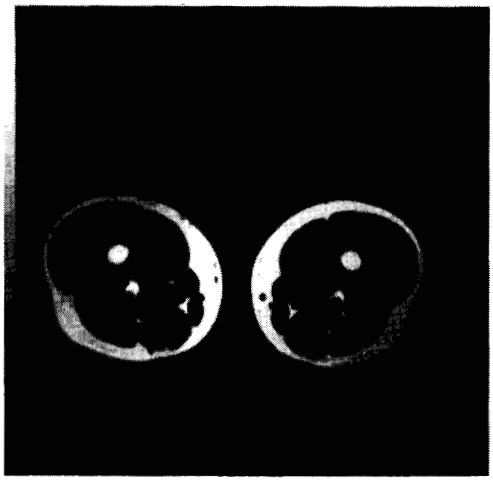

(c)

Fig. 8. (a) Magnitude detection of an image of the legs with water and lipid components in quadrature. (b) Synchronous detection of the in-phase component (water) of the same image. (c) Synchronous detection of the quadrature component (lipid).

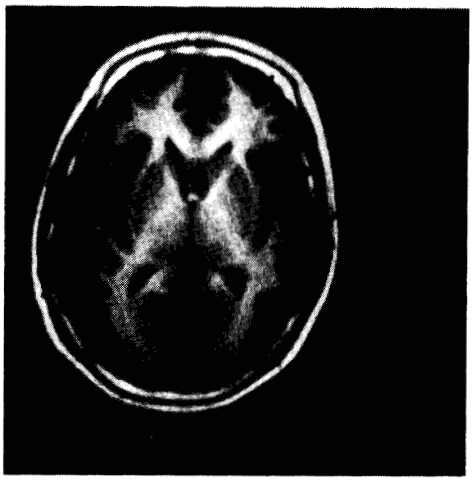

(a)

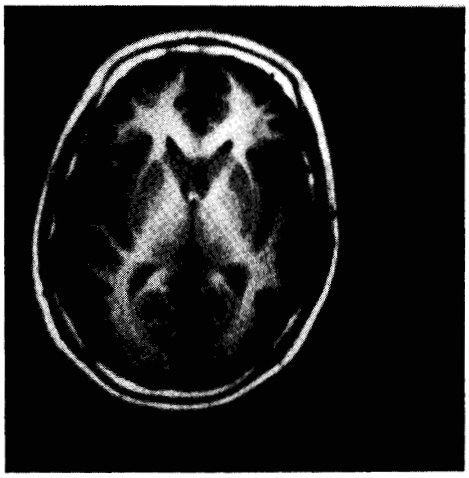

(b)

Fig. 9. (a) Magnitude detection of an inversion-recovery image of the head showing false levels for gray matter and reduced gray–white matter contrast. (b) Synchronous detection of the same image showing gray matter restored to the correct levels.

IV. Conclusion

Synchronous detection is used in amplitude modulation communication systems in several situations where envelope or magnitude detection is either inappropriate or inferior. Synchronous detection can also be used in MR imaging systems in place of the magnitude detection to provide complete suppression of undesired quadrature components, to preserve polarity and phase information, and to eliminate the biases and reduction in SNR and contrast in low SNR images. The incidental phase variations in the image are removed through the use of a homodyne demodulation reference, a reference that is "self-derived." The low frequency nature of this incidental phase allows, in many cases, the use of a low-pass filtered version of the original image as the demodulation reference. In other cases, the reference must be acquired separately,

but again due to the low frequency nature of the phase, the reference can be low resolution requiring only a few phase encodes. Additionally, since the reference does not need any diagnostic information, short repetition times and little averaging can further reduce acquisition times for the reference.

Synchronous homodyne detection has been applied to several situations in MR imaging where magnitude detection would result in image degradation due to noise or quadrature terms or loss of phase or polarity information. Low SNR images can be demodulated to remove the noise and signal dependent bias and improve SNR and contrast. Homodyne detection in partial k-space images removes the blurred quadrature terms arising from incomplete k-space. Water and lipid signals, when placed in quadrature, can be simultaneously collected and detected, and polarity in inversion-recovery signals can be preserved with a synchronous homodyne detector. In these applications where magnitude detection is inappropriate or performs poorly, homodyne detection has been shown to be a robust method of detecting and presenting MR images.

REFERENCES

[1] M. O'Donnell and W. A. Edelstein, "NMR imaging in the presence of magnetic field inhomogeneities and gradient field nonlinearities," *Med. Phys.*, vol. 12, pp. 20–26, 1985.

[2] C. H. Meyer and A. Macovski, "Square spiral fast imaging: Interleaving and off-resonance effects," in *Proc. 6th Ann. Meet. Soc. Mag. Res. Med.*, 1987, p. 230.

[3] A. Macovski and D. C. Noll, "Homodyne detection for improved SNR and partial k-space reconstructions," in *Proc. 7th Ann. Meet. Soc. Mag. Res. Med.*, 1988, p. 815.

[4] ——, "Applications of homodyne detection using separate reference acquisition," in *Proc. 7th Ann. Meet. Soc. Mag. Res. Med.*, 1988, p. 983.

[5] A. B. Carlson, *Communication Systems*. New York: McGraw-Hill, 3rd ed., 1986.

[6] R. E. Ziemer and W. H. Tratner, *Principles of Communications*. Boston: Houghton-Mifflin, 1976.

[7] D. Middleton, *An Introduction to Statistical Communication Theory*. New York: McGraw-Hill, 1960.

[8] H. Taub and D. L. Schilling, *Principles of Communication Systems*. New York: McGraw-Hill, 2nd ed., 1986.

[9] M. A. Bernstein, D. M. Thomasson, and W. H. Perman, "Improved detectability in low signal-to-noise ratio magnetic resonance by mean of a phase-corrected real reconstruction," *Med. Phys.*, vol. 16, no. 5, pp. 813–817, 1989.

[10] S. O. Rice, "Statistical properties of a sine-wave plus random noise," *Bell Syst. Tech. J.*, vol. 27, pp. 109–157, 1948.

[11] G. A. Wright and A. Macovski, "Computing material-selective projection images in MR," *Mag. Res. Med.*, vol. 11, pp. 135–151, 1989.

[12] P. Margosian, F. Schmitt, and D. Purdy, "Faster MR imaging: Imaging with half the data," *Health Care Instrumentat.*, vol. 1, pp. 195–197, 1986.

[13] D. A. Feinberg, J. D. Hale, J. C. Watts, L. Kaufman, and A. Mark, "Halving MR imaging time by conjugation: Demonstration at 3.5 kG," *Radiology*, vol. 161, pp. 527–531, 1986.

[14] D. G. Nishimura, A. Macovski, J. I. Jackson, B. S. Hu, C. A. Stevick, and L. Axel, "Magnetic resonance angiography by selective inversion recovery using a compact gradient echo sequence," *Mag. Res. Med.*, vol. 8, pp. 96–103, 1988.

[15] D. G. Nishimura, D. C. Noll, G. H. Glover, and A. Macovski, "Partial k-space reconstruction for magnetic resonance angiography by selective inversion recovery," in *Proc. Ann. Int. Conf. IEEE Eng. Med. Biol. Soc.*, 1989, p. 593.

[16] J. Cuppen and A. van Est, "Reducing MR imaging time by one-sided reconstruction," *Mag. Res. Imaging*, vol. 5, pp. 526–527, 1987.

[17] C. H. Oh, S. K. Hilal, J. B. Ra, and Z. H. Cho, "Faster magnetic resonance imaging by use of 3-quarter matrix data," in *Proc. 6th Ann. Meet. Soc. Mag. Res. Med.*, 1987, p. 455.

[18] J. R. MacFall, N. J. Pelc, and R. M. Vavrek, "Correction of spatially dependent phase shifts for partial Fourier imaging," *Mag. Res. Imaging*, vol. 6, pp. 143–155, 1988.

[19] J. C. Ehrhardt, Z. Tian, and W. Chang, "Reduced MR acquisition time with the CROCUS technique," *J. Comput. Assist. Tomogr.*, vol. 12, no. 3, pp. 468–473, 1988.

[20] R. J. Ordidge, A. Howseman, R. Coxon, R. Turner, B. Chapman, P. Glover, M. Stehling, and P. Mansfield, "Snapshot imaging at 0.5T using echo-planar techniques," *Mag. Res. Med.*, vol. 10, pp. 227–240, 1989.

[21] R. N. Bracewell, *The Fourier Transform and Its Applications*. New York: McGraw-Hill, 2nd ed., 1978.

[22] G. M. Glasford, *Fundamentals of Television Engineering*. New York: McGraw-Hill, 1955.

[23] J. L. Patrick, E. M. Haacke, and J. E. Hahn, "Water/fat separation and chemical shift artifact correction using a single scan," in *Proc. 4th Ann. Meet. Soc. Mag. Res. Med.*, 1985, p. 174.

[24] Z. Paltiel and A. Ban, "Separate water and lipid images obtained by a single scan," in *Proc. 4th Ann. Meet. Soc. Mag. Res. Med.*, 1985, p. 172.

[25] C. B. Ahn, S. Y. Lee, O. Nalcioglu, and Z. H. Cho, "Spectroscopic imaging by quadrature modulated echo time shifting," *Mag. Res. Imaging*, vol. 4-S1, pp. 110–111, 1986.

[26] W. T. Dixon, "Simple proton spectroscopic imaging," *Radiology*, vol. 153, pp. 189–194, 1984.

[27] Y. S. Kim, C. W. Mun, and Z. H. Cho, "Chemical-shift imaging with large magnetic field inhomogeneity," *Mag. Res. Med.*, vol. 4, pp. 452–460, 1987.

[28] I. R. Young, D. R. Bailes, and G. M. Bydder, "Apparent changes of appearance of inversion-recovery images," *Mag. Res. Med.*, vol. 2, pp. 81–85, 1985.

[29] C. J. Bakker, C. N. de Graaf, and P. van Dijk, "Restoration of signal polarity in a set of inversion-recovery NMR images," *IEEE Trans. Med. Imaging*, vol. MI-3, pp. 197–202, 1984.

[30] H. W. Park, M. H. Cho, and Z. H. Cho, "Real-value representation in inversion-recovery NMR imaging by use of phase correction method," *Mag. Res. Med.*, vol. 3, pp. 15–23, 1986.

[31] J. A. Borrello, T. L. Chenevert, and A. M. Aisen, "Regional phase correction of inversion-recovery MR images," *Mag. Res. Med.*, vol. 14, pp. 56–67, 1990.